Accepted Manuscript

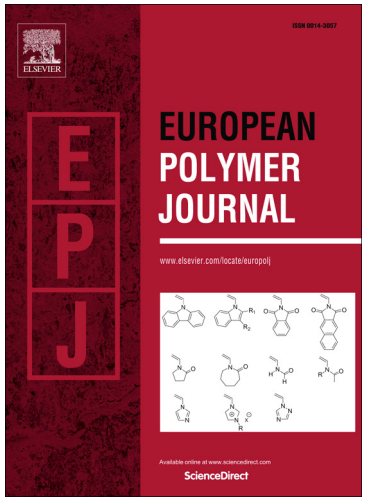

Quantitative and mechanistic analysis of impact of novel cassava-assisted improved processing on fluid transport phenomenon in humidity-temperature-stressed bio-derived films

K.S. Tumwesigye, J.C. Oliveira, M.J. Sousa-Gallagher

PII: S0014-3057(16)31491-4
DOI: http://dx.doi.org/10.1016/j.eurpolymj.2017.04.027
Reference: EPJ 7839

To appear in: *European Polymer Journal*

Received Date: 11 November 2016
Revised Date: 13 April 2017
Accepted Date: 19 April 2017

Please cite this article as: Tumwesigye, K.S., Oliveira, J.C., Sousa-Gallagher, M.J., Quantitative and mechanistic analysis of impact of novel cassava-assisted improved processing on fluid transport phenomenon in humidity-temperature-stressed bio-derived films, *European Polymer Journal* (2017), doi: http://dx.doi.org/10.1016/j.eurpolymj.2017.04.027

Quantitative and mechanistic analysis of impact of novel cassava-assisted improved processing on fluid transport phenomenon in humidity-temperature-stressed bio-derived films

K.S. Tumwesigye[1, 2], J.C. Oliveira[1], M.J. Sousa-Gallagher[1*].
[1]Process and Chemical Engineering, School of Engineering, University College Cork, Cork, Ireland
[2]National Agricultural Research Laboratories, NARO, Kawanda, Uganda
*m.desousagallagher@ucc.ie

Abstract

Bio-derived films' realistic performance integrity is ascertained by their resilience in highly-stressful storage conditions, a function of its ability to respond timely and manages fluid barrier appropriately. Bio-derived films' moisture and temperature sensitivity often posed mass transport challenges, thus decreasing their lifespan. Quantifying bio-derived film mass transport behaviour has been limited to mass transfer representations, which can be imperfect to understand fully mass transport phenomenon. This study reported quantitative and mechanistic analysis of fluid-phase mass transport phenomenon in Simultaneous Release Recovery Cyanogenesis-produced intact bitter cassava (IBC) bio-derived films under stressful conditions. Films were tested for solvent solubility, swelling ratio, sorption and permeability to water vapour and oxygen at 10-40°C and 10-95% RH. Film's structural alterations were characterised by their thermal and chemical properties. Modified-BET, Peleg, Oswin models best described sorption data. Temperature-dependence of film water vapour permeability was simulated best by Arrhenius model, while oxygen permeability was influenced highly by crystallinity and RH. Non-organic and organic film-solvent diffusion followed case II and Fickian diffusional patterns respectively. Solvents induced structural changes in IBC films with concentration-dependent diffusion. Cassava bio-derived films' integrity will depend on the host environment, thus maximum care should be ensured to minimise environment impact during applications. Nonetheless, IBC films hold potential as biomaterials for broad range product use.

Key words: Mechanistic; Cassava film; Mass transport; Fickian diffusion; Temperature-RH-dependence

Nomenclature

A	film area exposed to water permeation (m^2)	R^2	Coefficient of determination
a_w	water activity of the environment surrounding the film	s	slope
D	permeation coefficient at a given absolute temperature ($g.mm.m^{-2}.d^{-1}.kPa^{-1}$)	t	sampling time (min)
D_0	pre-exponential factor-the permeation coefficient (basic parameter) ($g.mm.m^{-2}.d^{-1}.Pa^{-1}$)	T	absolute temperature (K)
E_a	activation energy for permeation (kJ/mol)	V_d	volume of dry film (ml)
EMC	proportion of moisture adsorption in the film at predetermined temperature and relative humidity, and at constant pressure (%)	VR	Regression variance
FS_{ol}	solvent solubility in film (mg ml^{-1})	V_s	molar volume of solvent (cm^3 mol^{-1})
FS_{tm}	saturation swelling ratio of wet film (%)	W_f	weight of the film (g)
k	kinetic constant	W_s	weight of solvent in the film (μg)
m	weight of wet film at equilibrium due to water vapour permeation (g)	$X_{i(o)}$	observed equilibrium moisture content (%)
M	mass sorption of solvent in the film (mg)	$X_{i(P)}$	modelled equilibrium moisture content (%)
M_d	weight of dry film (g)	β	lattice constant
M_{eq}	total weight of wet film at equilibrium	δ_f	solubility parameter of the film
M_f	molecular weight between cross-links (g)	δ_l	film thickness (mm)
M_i	mass of wet film equilibrated for 48 h at predetermined temperature and relative humidity, and constant pressure (g)	δ_s	solubility parameter of the solvent
m_o	weight of film before permeation experiment (g)	ε	square absolute deviation between observed and modelled equilibrium moisture
M_{tm}	saturated weight of wet film (g)	Σ	summation
N	number of experimental points	ln	Natural logarithm
n	kinetic exponent	ρ	mean relative deviation modulus (%)
P_w	film permeability coefficient ($g.mm.m^{-2}.d^{-1}.Pa^{-1}$)	ρ_f	film density (g m^{-1})
P_s	partial pressure of water saturation at temperature considered (Pa)	χ	film-solvent interaction parameter
R	universal gas constant ($Jmol^{-1}K^{-1}$)	ϕ_f	swollen film volume fraction

1. Introduction

Cassava biobased films (CBF) are widely produced to replace non-biodegradable plastics for broad range functional applications such as guarding food and non-food products against physical, chemical and microbiological hazards throughout the distribution chains [1, 2]. The advantages of CBF are comparable to the current polymer food packages (PFP) [3]. The CBF have potential biodegradability, and can be destroyed by natural processes, leaving no byproduct waste, to ensure green environment [3]. Environmental-destroying and high energy processes (e.g. toxic fume emission enhancer pyrolysis), associated with PFP [4] are not required for CBF. Further, CBF excellent film forming properties, ease of forming packages, as well as their economically-cost effective material source and development, present high potential for CBF to be produced on a large industrial scale [5]. However, the main disadvantage of CBF is limited long-life properties (e.g., resistance to chemical reactions), requiring more research efforts for it to replace PFP [5, 6].

As industrial demand for CBF becomes a reality, it is expected that these materials will be applied at different temperatures and relative humidity (RH). Highly variable temperature and RH is the main physical threat, along the distribution chain, that enhances chemical and microbiological risk to products [7], and thus create challenges to the development of suitable bioderived materials. In particular, biobased materials are sensitive to moisture fluctuations [8, 9] and solvents, which in turn can influence their barrier and protective properties due to changes in structural characteristics. Thus, an understanding of the physico-chemical resilience nature of the CBF will play a crucial role in development of sustainable industrial applications with technical and commercial impact. These materials can be protective coatings and films, modified atmosphere packaging and active packaging that ensure environmental protection and product integrity. This can be achieved by quantifying the transport phenomenon, through dissecting its mechanisms that underlie fluid (moisture vapour, gas) transfer and solvent diffusion in CBF. Although research on fluid transport mechanisms through biobased materials remain inconclusive, it is widely known that fluid transport through polymer membranes is largely a function of: (i) solubility, permeability and diffusivity [10, 11]; and (ii) material composition, structure and mechanical properties [12, 13]. Unlike in commercial materials utilizing liquid solvents, a unified approach to quantity and describe the complex mechanisms of mass transport in biobased packaging materials is still shaky. As the application integrity issues of packages become more apparent, so are the requirements to develop novel materials and precise methods that ensure proper regulation of barrier, resistance and protective properties across differentiated environmental conditions in the distribution chain.

The barrier properties of packages are commonly determined by applying existing fundamental empirical mathematical models. Several model references for describing effect of temperature and relative humidity on moisture adsorption and permeability to water vapour and oxygen have been widely used in different films [14-16]. Models for sorption isotherms include diffusion-adsorption equation that eliminates thickness effect in assessing adsorption of hydrophilic films [17]. Other models related to sorption-diffusion and solubility are also described using Fickian theories [18-20]. Sorption isotherms for cassava were evaluated using Peleg model in flour film [21]; BET, GAB, Henderson and Oswin models for starch and soy protein concentrate edible films [22, 23]. The water vapour and oxygen/carbon dioxide transmission rates as function of temperature are often described by fitting the data to Arrhenius model [24]. The models described above are only quantitative representations that use concentration-time and mass flux-time curves to describe mass transfer behaviour of

solvents through film membranes [25, 12, 26]. Alternative mechanical assessment techniques that provide useful insights into underlying mechanisms of processes have been applied in understanding the dissolution behaviour of crystals under the influence of ionization and micellar solubilisation [27], modelling mass balances, flux capacity, fluid permeation through compressible fibre beds [28] and reaction directionality constraints to predict fluxes through metabolism [29]. Recently, the contribution of seals to the permeability of thermo-sealed packages has been quantified, showing approximately 25 % of the system total mass transfer [30]. Taken together, the quantitative and mechanistic approaches can be used to describe properly the mass transport phenomenon and provide avenues in CBF development and widened applications.

Although quantitative assessment has been significantly used to understand the barrier properties of polymeric materials (PM), little has been done to assess fluid transport mechanisms through PM in stressed temperature, relative humidity and different solvent environments. This may be partly due to the limited research validation of PM under realistic natural conditions and under use environments. Furthermore, there are still scarce literature reports about the quantitative evaluation of effect of temperature and relative humidity on the barrier properties of CBF. Moreover, the insignificant validation research under realistic conditions is largely shared by CBF. Starch, in combination with natural fibres, is often used to manufacture whole bio-based composites. While there are direct benefits to use natural fibres in composites, their performance is often very nonlinear, due to their highly sensitivity to moisture and temperature [9].
Recently, a combination of a novel bitter cassava (BC) material and an improved simultaneous release recovery cyanogenesis (SRRC) processing methodology resulted into development of new low-cost biobased film, which demonstrated potential use in food packaging [3]. In order to develop sustainable materials with efficient barrier properties and organic solvent resistance, an understanding of the association between structural characteristics of BC and underlying mechanisms that define fluid mass transport phenomenon as well as their quantification is necessary.

While poor barrier properties are often associated with hydrophilic nature of CBF, their limited validation in realistic conditions, as well as the quantitative analyses that disregard underlying mass transport mechanisms under highly variable relative humidity and temperature, influence package use. The objective of this study was to: i) determine moisture sorption characteristics as well as permeability to water vapour and oxygen of intact bitter cassava films; ii) evaluate the relevance of the various models in predicting barrier performances in simulated realistic conditions of different relative humidity for specific storage temperature; iii) provide an understanding of the mechanism of mass transport phenomena of water vapour, oxygen and organic solvents through the film using relevant models which relate to solubility, diffusion and adsorption laws; and iv) relate models to the film structural (chemical and thermal) characteristics, determined using Fourier Transform Infrared (FTIR) and Differential Scanning Calorimetry (DSC). This was done in order to assess the adequacy of the models to predict nature of mass transport, and the time-dependent behaviour, and impact, of novel BC and SRRC. Also, to elucidate the relationship between transport properties and SRRC-induced polymer structural changes.

2. Materials and methods

2.1 Materials

Films were produced by solution casting using the procedure reported by Tumwesigye et al. [3]. Mixtures of cassava BPD (3 % w/v) and glycerol (30 % w/w) were heated at 70^{0}C for 25 minutes. Prior to moisture barrier characterisation, films were conditioned at 23 ± 2^{0}C and 54 %RH. Thickness was measured in six different locations using an absolute digital Calliper (Digmatic, Mitutoyo UK Ltd).

2.2 Mass transport characterisation

2.2.1 Moisture barrier (MB)

The MB characteristics were determined in terms of moisture adsorption (MA) and water vapour permeability (WVP).

Determination of MA characteristics was done by creating an environment of specific relative humidity with glycerol solution (0 % to 100 % v/v). Various methods of creating specific relative humidity environments such as saturated salt solutions have been proposed [31]. However, glycerol was preferred due to its lone advantage and ease in making 0 – 100 % v/v solutions that are cheap, non-corrosive and do not vary with temperature changes.

Film strips (3 x 1.5 cm) were pre-dried until attaining constant weights, achieved at 90^{0}C for 9 h. Film MA was determined at 10, 20 and 30^{0}C, and 10-90 %RH in controlled chambers and the final moisture content (EMC) calculated, on a dry basis, according to Eq. 1.

Eq. 1: Equilibrium moisture content, %

$$\text{EMC}, \% = \left(\frac{M_i - M_d}{M_d}\right) 100$$

$M_{i:}$ weight of wet film equilibrated for 48 h at predetermined temperature and relative humidity, and at constant pressure

$M_{d:}$ weight of dry film after oven-drying at 105^{o}C, 29 h

The WVP was determined according to ASTME [32] method at 10, 20, 30, 40°C and at RH gradients across the film of 75, 85 and 95 % using Eq. 2.

Eq. 2: WVP determination

$$m = m_0 + \frac{P_w}{\delta_l} * A * P_s \left(a_{w_1} - a_{w_2}\right) t$$

m:	film weight at time t
m_o:	initial film weight
P_w:	film permeability coefficient
δ_l:	film thickness
A:	film area exposed to permeation
P_s:	partial pressure of saturation at temperature considered (1 kPa)
a_w:	water activity of the environment with a_{w1} = 1 and a_{w2} = 0 corresponding with 0-100% relative humidity

The detailed procedure was followed based on Tumwesigye et al. [3] without changes. The simplified diagram of the WVP test system is shown in flow diagram 1. Concisely, films

strips (7.4 cm diameter) were mounted on acrylic cells and hermetically sealed around the open transfer zone. Calcium chloride and salt solution were used to create 0-75, 0-85, 0-90 %RH gradient between inside the cells and outside hermetically sealed chambers respectively. Weights were taken after every 2 h for 10 h. The breakthrough permeation time (10 h) was determined as the point when the solvent begins to gel the calcium chloride in the permeation cell. Results were expressed in gmm/m² d kPa).

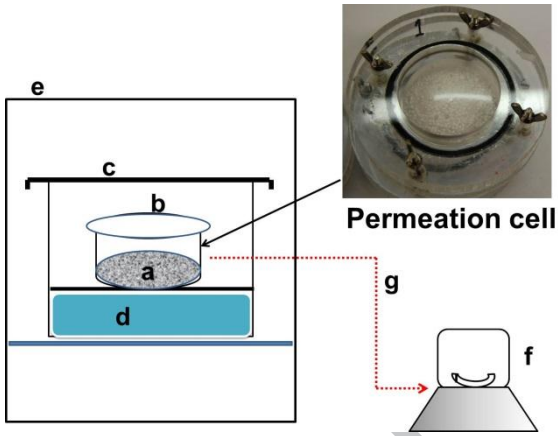

Flow diagram 1. A schematic diagram of the permeation system. Letters represent calcium chloride at a_w 0 (a); film strip mounted on top of the cell (b); airtight chamber /container (C) containing solution at given relative humidity (d); temperature controlled chamber (e); analytical weigh balance (f); and permeation cell transfer route to the balance (g).

2.2.2 *Gas barrier*

The gas barrier characteristics were determined in terms of permeability to oxygen (PO_2). The PO_2 was measured following the method described by Abdellatief et al. [33] and reported in Tumwesigye et al. [3] without significant modifications using a PBI Dansensor (CheckMate 9900, USA). The PO_2 was determined at the temperature of 10, 20, 30 and 40^{0}C and RH gradient of 0-75, 0-85 and 0-95 %. The possible leakage within testing chambers was tested with an empty chamber and found to lie within minimum mean limits (1.5 x 10^{-3} cm^3 .mm/(m^2 .day.kPa). Triplicate tests were considered and mean values for calculating PO_2 expressed as cm^3 .mm/(m^2 .day.kPa).

2.2.3 Fluid barrier modelling

The MA data were fitted to eight models (Table 1S) in order to describe adsorption isotherms in the 10-30ºC, and correlate equilibrium moisture content and relative humidity. Model parameters were estimated by non-linear regression procedure using Excel (2010) solver and goodness of fit evaluated by (Eq. 3) and (Eq. 4). Accurate mathematical description of isothermal was considered when ρ≤5 %, VR≤5% and R^2≥0.99 across the experimental temperature range.

Eq. 3: Mean relative percentage deviation modulus, ρ, %

N:	number of experimental points
ε:	square absolute deviation
(p) and (o):	modelled and observed
$X_{i(o)}$:	Observed equilibrium moisture content

$$\rho,\% = \frac{100}{N}\ \Sigma_{i=1}^{N} \frac{|\varepsilon_i|}{X_{i(o)}}$$

$X_{i(P)}$	modelled equilibrium moisture content

Eq. 4: Regression variance, VR

$$\mathrm{VR} = \Sigma_{i=1}^{N} \frac{\left|X_{i(p)} - X_{i(o)}\right|^2}{N-1}$$

2.2.4 Film solubility (FS_{ol}) and swelling ratio (FS_{tm}) measurements

The film solubility (FS_{ol}) and swelling ratio (FS_{tm}) measurements were conducted gravimetrically using an electronic balance (Sartorius, Cubis MSA, Germany) with a 0.1 mg resolution. Initially, a pre-weighed and laboratory fumehood-dried (1.0 % moisture content) films were immersed in 100 ml of water at 40^{o}C, 75 % & 95 % RH). The wet film was removed from water after every 10 min until 60 min, pre-dehydrated on filter paper and quickly weighed on the balance. The process of withdraw was maintained within 60 s to minimise any difference in weights of different film portions. Seven (7) similar film portions were used, each withdrawn from water sequentially at an accumulated time, weighed and discarded. This was done to avoid interruptions of water diffusion and film swelling processes during transfers between water and electronic balance. The same experiment was conducted with organic (Toluene) and inorganic (Paraffin oil) solvents. Triplicate measurements were considered for the purposes of reproducibility of the experimental results. The FS_{ol} and FS_{tm} were estimated as described in Chen et al. [25] using Eqs. 5 and 6.

Eq. 5: Film solubility, FS_{ol}

$$\mathrm{FS_{ol}} = \frac{\mathrm{M_{eq} - M_d}}{\mathrm{V_d}}$$

Eq. 6: Swelling ratio

$$\mathrm{FS_{tm}},\% = \left(\frac{\mathrm{M_{tm} - M_d}}{\mathrm{M_d}}\right) 100$$

FS_{ol}:	solvent solubility in the film
M_{eq}:	total weight of wet film at equilibrium (eq)
M_d:	weight of dry film
V_d:	volume of dry film
FS_{tm}:	saturation swelling ratio of wet film
M_{tm}:	saturated weight of wet film

The FS_{tm}, V_d and film density (F_d) were determined as described in Chen et al. [25]. It is noted that film V_d was 1, and thus F_d was equal to its solubility. The FS_{ol} and FS_{tm} experiments were conducted at 25^{o}C.

2.2.5 Organic and inorganic solvent permeation and sorption tests

Organic and inorganic solvents are encountered in the supply chain of the materials, and their evaluation could provide an understanding of how IBC materials will behave when subjected to these solvents. Thus, a purposive experiment with toluene and paraffin oil was conducted, as illustrated in flow diagram 2. This design comprised two sections: the first upper section (Flow diagram 2) was meant for measuring solvent vapour sorption through the film strip (F) placed on top of wire gauze (G) that allows free movement of vapours (V) from solvent (S) to permeate through the film. The second section allows for measuring the permeability of the sorbed film (f) obtained from the upper section. Solvent vapour sorption test was accomplished by allowing the vapours to go through pre-weighed film disc of 19.6 cm^2 permeation area. The films were withdrawn every 10 min, and their weights taken using the electronic balance, B (Sartorius, Cubis MSA, Germany). To ensure reliability, three film

samples, making the replicates, were tested for specific measuring time, and transferred for permeation tests.

The solvent vapour permeation was conducted concurrently with the vapour sorption one by hanging the sorbed film of specific test time every 10 minutes, as shown in Flow 2. The amount of solvent permeated through the film was taken as the difference in loss of weight, which is equivalent to solvent released from the films. Thus, a weight loss-time (mass flux-time) plot was derived, and an instantaneous mass uptake was obtained by extrapolating the linear regression curve back to zero [25].

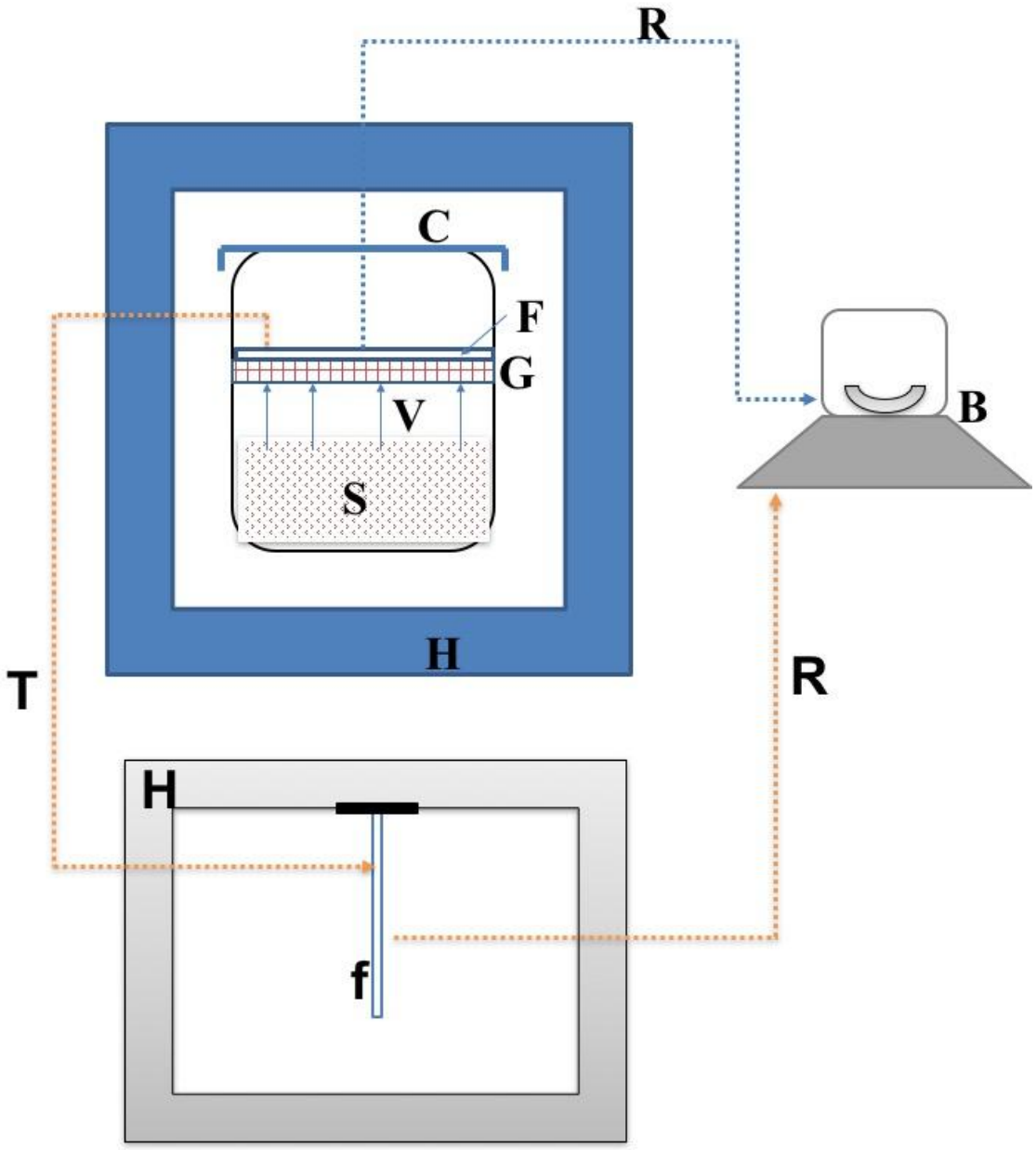

Flow diagram 2: A schematic diagram of the permeation system for solvent permeation measurements (S). Letters represent solvent vapour (V); film strip (F) mounted on top of the perforated gauze (G), placed inside an airtight chamber /container (C), stored in a

temperature regulation chamber (H). T, R and f represent solvent permeated film to drying chamber, transfer of film to weighing scale (B) and film for permeation experiment respectively.

The sorption and permeation tests were carried out at 25^0C, temperature being controlled by the chamber, H. All the weights were taken within 60 s.

2.2.6 Statistics

Data analysis was performed by Statistica 7.1 software (StatSoft Inc., Tulsa, USA) and Microsoft Excel, version 2013 to determine if RH and T has significant impacts on MB and GB, evaluate the goodness of fit of each model, the coefficient of determination and the mean relative percentage deviation modulus. Where mean values were used, errors bars were provided for comparison purposes. Differences were considered to be significant when $p \leq 0.05$.

2.3 Models and conceptual background

The mass transport behaviour of fluids (moisture and gas) through polymeric films is preferably assessed by considering models that adequately fit the empirical data., e.g. rate of mass sorption [34], sorption-diffusion [35], film swelling and film-moisture interaction [36], gas permeability, diffusivity and solubility [37], and temperature-sorption-permeation [38]. The entire above plus adsorption models (Table.1) are used to assess the mass transport behaviour in this study.

2.3.1 Arrhenius model

Like any other materials, biobased materials' permeability to water vapour and gases is a function of temperature, and thus described by Arrhenius equation (Eq. 7) (Arrhenius, 1889).

Eq. 7: Arrhenius model

$$D = D_0 . e^{\frac{E_a}{RT}}$$

Eq. 8: Linearising Eq. 7
by transforming it into logarithmic form

$$\ln[D] = \ln[D_0] - \frac{E_a}{R} \cdot \frac{1}{T}$$

D:	permeation coefficient at temperature T ($g.mm.m^{-2}.d^{-1}.Pa^{-1}$)
D_0:	pre-exponential factor-the permeation coefficient (basic parameter) ($g.mm.m^{-2}.d^{-1}.Pa^{-1}$)
E_a:	activation energy for permeation (kJ/mol)
T:	absolute temperature (Kelvin); and R, universal gas constant ($Jmol^{-1}K^{-1}$)
ln:	natural logarithm

By plotting ln[D] vs 1/T, a linear curve is obtained. By regression analysis of the straight line, y = sx + c, a slope, s is obtained, and $\ln[D_0]$ represents the intercept, y. Thus, E_a can be calculated from Eq. 9.

Eq. 9: Activation energy

$$E_a = -s \cdot R$$

2.3.2 Analysis of film–solvent interaction

Biobased films swell when they are exposed to solvents, and the degree of swelling is a function of the length of the network chain, temperature, type of solvent and strength of thermodynamic interaction between the film chains and solvent molecules [39]. To assess the effect of SRRC and bitter cassava on the film molecular structure and possible modifications, which are pertinent factors that can influence barrier properties, the Flory-Huggins equation (Eqn. 10) [40] was applied. The thermodynamic parameters evaluated here include film volume fraction (ϕ_f) (Eq. 11.), solvent volume fraction, film-solvent interaction (χ), and film mass between possible crosslinks (M_f).

Eq. 10: Flory-Huggins equation

$$\frac{1}{M_f} = \frac{\emptyset_f + \chi\emptyset_f^2 + \ln(1-\emptyset_f)}{\rho_f V_s\left(\emptyset_f^{\frac{1}{3}} - \frac{1}{2}\emptyset_f\right)}$$

Eq. 11: Film volume fraction (ϕ_f)

$$\emptyset_f = \frac{1}{1+q}$$

M_f: molecular weight between cross-links [reciprocal of moles of cross-linked units per unit film weight (g)]
ϕ_f: swollen film volume fraction
χ: film-solvent interaction parameter
ρ_f: film density; and
V_s, solvent molar volume

W_s: weight of solvent in the film
W_f: weight of the film
β: lattice constant (0.34)
V_s: solvent molar volume
R: universal gas constant
T: absolute temperature
δ_s & δ_f:solubility parameters of solvent and film

Considering solvent soluble polymers (e.g. cassava film), q was further segregated into $q = W_s/W_f$.

Furthermore, χ was calculated according to Bristow & Watson [41] using Eqn. 12, and described in Barlkani & Hepburn [42].

Eq. 12: Computing film-solvent interaction parameter

$$\chi = \beta + \left(\frac{V_s}{RT}\right)\left(\delta_s - \delta_f\right)^2$$

The δ_f was derived by immersing film in water and quantifying the loss within 24 h, while δ_s were obtained from [43].

2.3.3 Film solvent sorption and permeation theory and mechanism

The solvent vapour diffused through the film for sorption test, whereas the diffusional movement of solvent vapour outer at film surfaces was unidirectional across film thickness for the permeation test. Applying the assumptions: i) perpendicular diffusional flow; ii) insignificant pressure flux variation; and iii) concentration gradient as driving force, Ritger and Peppas empirical equation (Eq.13) [34] was used to express solvent transport behaviour in BC films, as the mass sorption against time. In addition, since the experiment was conducted in specific conditions of temperature and RH, isothermal conditions were assumed.

Eq. 13: Power equation

$M = kt^n$

M:	mass sorption of solvent in the film at a given time (t)
k:	kinetic constant (mass sorption rate)
n:	diffusional (kinetic) exponent

The n is an indication of the solvent transport mechanism. For Fickian diffusion, n = 0.5, and non-Fickian diffusion, n > 0.5 (n = 1, case II diffusion & 0.5 < n < 1.0, anomalous diffusion) [12], and this was determined from the total mass absorbed. According to Fickian and non-Fickian diffusional adsorption through a thin film (Eqn. 13), applies to only 60 % of the process, and this was used (in this study) to evaluate solvent diffusion in and out of the film in the permeation tests.

Since the thickness-to-radius ratio of films used (0.002) was < 0.2 [44], the neck-in (edge) effect (film thickness and width reduction) [45] was neglected, and the one-dimensional diffusion of water vapour and O_2 through the film was assumed for the permeation tests. Using the mass balances, the concentration-time (c-t) curves were developed and used in the description of mass transfer patterns.

2.4 Film structural characterisation

Thermal analysis of glass transition (T_g), melting (T_m) temperatures, crystallinity (CRY) and enthalpy change (ΔH), was conducted using a differential scanning calorimeter (DSC 200 F3) equipped with a thermal analysis data station. A hermetically sealed DSC pan with fresh derivative powder (10 mg), together with a reference empty pan were heated from 20 to 250°C at a rate of 10°C/min, cooled back rapidly to 20°C and reheated at a rate of 5°C/min to 250°C to give them thermal history. T_g, T_m, CRY and ΔH were calculated using the built in software and determined by considering the heat capacity change observed on the second heating.

Structural changes and modification due to mass transport phenomenon of solvents in films were characterised by using Fourier transform infrared spectroscopy (FTIR). This procedure was derived from Tumwesigye et al. [3]. A film strip was placed in the sample holder. The spectra were recorded with an UV/Vis spectrum one FTIR spectrometer (Perkin Elmer Lambda 35, USA), frequency range of 4000–400 cm^{-1} and $4cm^{-1}$ resolution in the transmittance and absorbance modes for individual spectrum with 30 scans at room temperature.

3. Results and discussion

3.1 Moisture barrier

The moisture adsorption isotherms at 10, 20, 30^0C for 10 - 90% RH are shown in Fig. 1. For Peleg model, intact bitter cassava films (IBC) follow a Type II isotherm, regardless of the temperature in question (Fig 1ai & aii), implying that these films possess wide pore size distributions leading to fluid pathways that are tortuous and highly variably. Additionally, the equilibrium moisture content (EMC) increased corresponding to increases of RH at constant temperature, perhaps due to the exposure of these films to higher quantities of moisture. Perhaps, this could also be due to water binding thus increasing mobility and dissociation

However, a relatively lower increase in EMC was observed when these films were exposed to higher temperatures at constant RH (Fig 1ai).

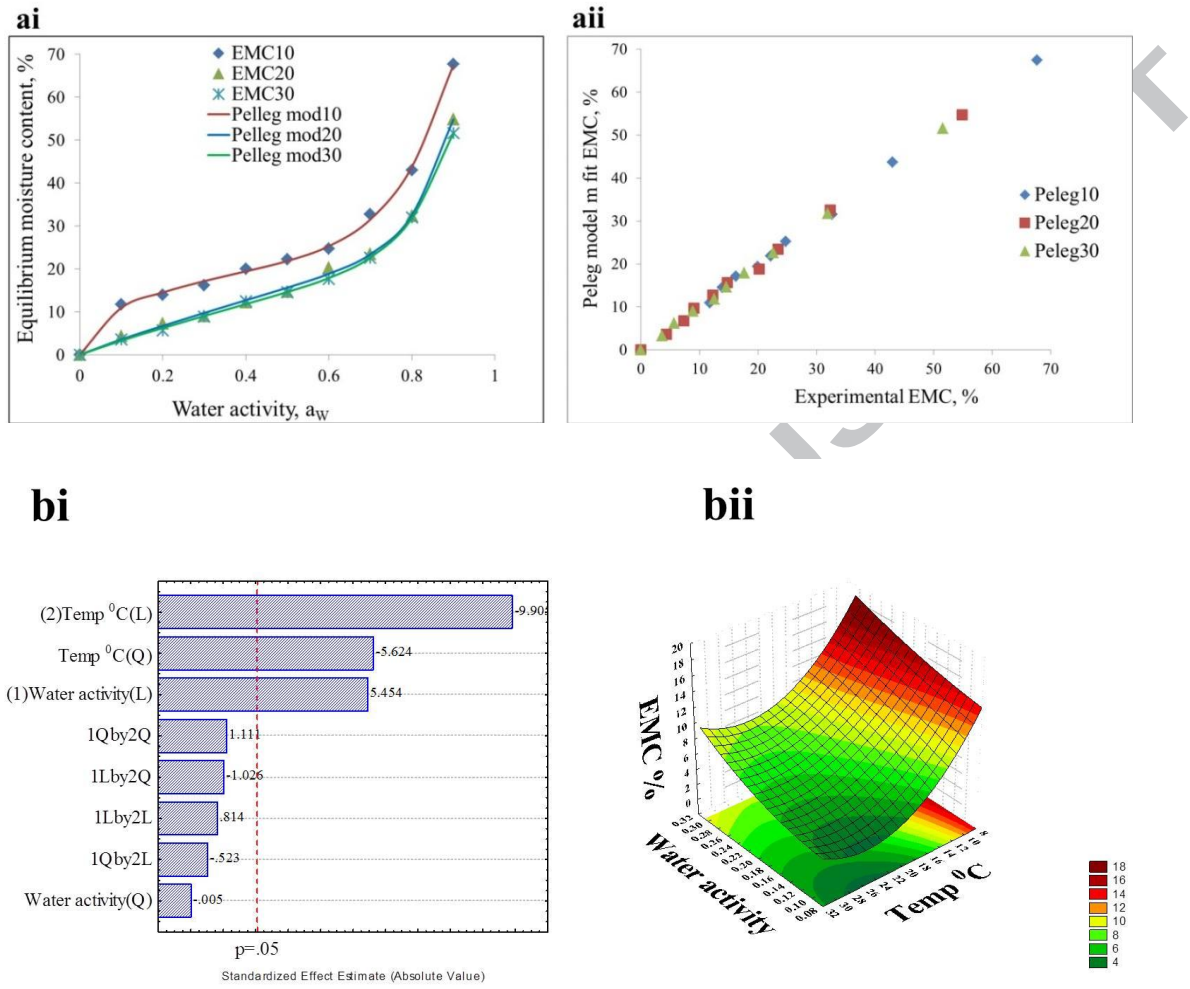

Fig 1. Moisture barrier properties shown by adsorption isotherms (a); effect of relative humidity and temperature on EMC (ai); and Peleg model fit for all temperatures (aii). Impact of water activity and temperature on equilibrium moisture content (EMC) shown by Pareto ANOA (bi) and surface plot (bii).

Statistically, Fig 1 bi showed that temperature had more impact on film adsorption of moisture than RH, both linearly and quadratically. It can be shown that a higher EMC was attained at low temperature (Fig 1 bii). This phenomenon can be explained by the fact that at lower temperatures, films moisture affinity is high with higher capacity adsorption. It could be also due to the faster mobility of water molecules at higher temperatures causing a decrease in the intermolecular attractive forces. Chowdhury et al. [46] reported that, at higher temperatures, water molecules move to higher energy levels, become less stable and break away from the binding sites of the materials thus decreasing the monolayer moisture content. Similar temperature dependent adsorption isotherms trends in biobased materials were observed elsewhere [22, 47].

Adsorption isotherms are often applied in industry to select suitable adsorbents during separation processes but also to select the best storage conditions of products in various environments. A number of models and the corresponding parameter adequacy to describe the above phenomena are presented in Table 1 S and Table 1. As shown, modified BET,

Peleg and Oswin models best described the relationship between EMC and water activity at each temperature (10, 20, 30°C) (Table 1) and under the conditions tested (10-90 % RH), with Peleg posting the most suitable model for IBC films.

The moisture barrier property of materials is essential to approximation and prediction of the product-package shelf-life, with a precise package system barrier requirement governed by the product characteristics and the targeted applications. Moisture regulation in packaging can cause negative changes in product quality and shelf-life, and change package material characteristics.

The effect of temperature on modelled model's EMC was assessed by an Arrhenius model (Eq. 8), and results presented in Table 1. Also, the same procedure permitted evaluation of the activation energy (Eq. 9).

Table 1

Model name	**T, °C**	**Fit quality**			**Arrhenius parameters**	
		ρ, %	**VR, %**	**R^2**	**E_a**	**P_o**
Ferro-Fontan	10	5.986	1.710	0.984		
	20	5.837	1.097	0.993	9.68	1.07
	30	9.123	0.857	0.987		
GAB	10	24.534	42.153	0.896		
	20	17.510	11.046	0.962	9.77	1.03
	30	23.474	11.720	0.956		
Halsey	10	4.805	1.142	0.983		
	20	8.272	1.278	0.990	10.97	1.38
	30	13.635	1.749	0.988		
Henderson	10	18.636	19.645	0.951		
	20	16.762	5.788	0.980	8.29	1.80
	30	15.477	3.764	0.986		
Modified BET	10	4.081	1.126	0.996		
	20	4.289	0.413	0.999	8.73	1.57
	30	3.421	0.285	0.999		
Oswin	10	9.578	5.029	0.988		
	20	4.007	0.726	0.998	8.73	1.57
	30	4.596	0.385	0.999		
Peleg	10	3.258	0.588	0.999		
	20	4.581	0.532	0.998	9.61	1.11
	30	3.131	0.120	1.000		
Smith	10	13.280	10.361	0.966		
	20				11.39	1.69

30	12.646	5.823	0.980
	11.593	3.883	0.985

ρ, mean relative deviation modulus; VR, standard error of estimate; R^2, coefficient of determination; E_a, activation energy; P_o , pre-exponential factor

The temperature dependence of WVP is presented in Fig. 2, showing increases in RH and temperature increased exponentially the IBC film permeability to moisture (Fig. 2a), statistically demonstrating that high significant ($p \leq 0.05$) impact was attained at higher RH and T (Fig 2b). As expected, the phenomenon is associated with molecular activation, causing film segment movement with formation of cavities that often facilitate movement of solvents through porous films [48]. There seemed to be less impact (p>0.05) of RH and T on WVP at 75% and 85% for 10ºC and 20ºC.

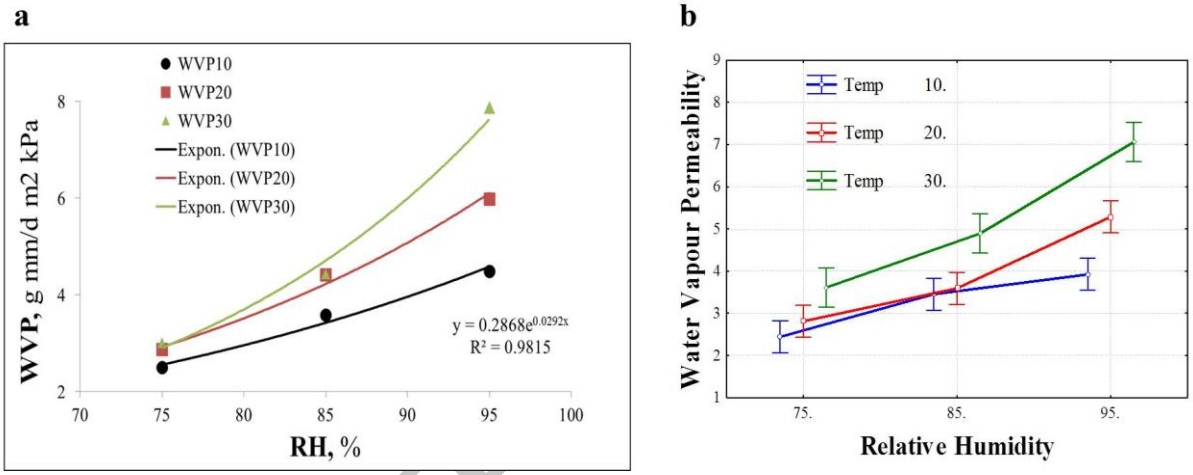

Fig 2 Water vapour permeability (WVP) dependency of temperature (T), showing exponential increases with relative humidity (RH) (a), significant effect of RH and T on WVP (b).

The temperature-dependence phenomenon is normally presented by an Arrhenius type association [38], and its model (Eq. 8) was used to predict behaviour of moisture permeation of IBC films (Fig 3 & Table 2). The increase in WVP suggests higher activation energy for moisture permeation (Table 2).

Table 2. Permeability and parameters of Arrhenius model fit

T, ºC	**Model WVP,** g.mm.m^{-2}.d^{-1}.Pa^{-1}			**P_O**
	P75 mod	**P85 mod**	**P95 mod**	
10	5.674± 0.19	6.699± 0.61	7.368± 0.31	283.80
20	5.673± 0.40	6.698± 0.76	7.366± 0.44	783.80
30	5.672± 0.40	6.697± 0.76	7.365± 0.44	4128.60
E_a, (Jmol^{-1})	10.51	12.21	15.87	

Pmod, permeation coefficients at 75, 85, 95% RH; P_O, pre-exponential factor; E_a, activation energy for permeation

The Arrhenius prediction of WVP as T increased from 10ºC to 30ºC is shown in Fig. 3.

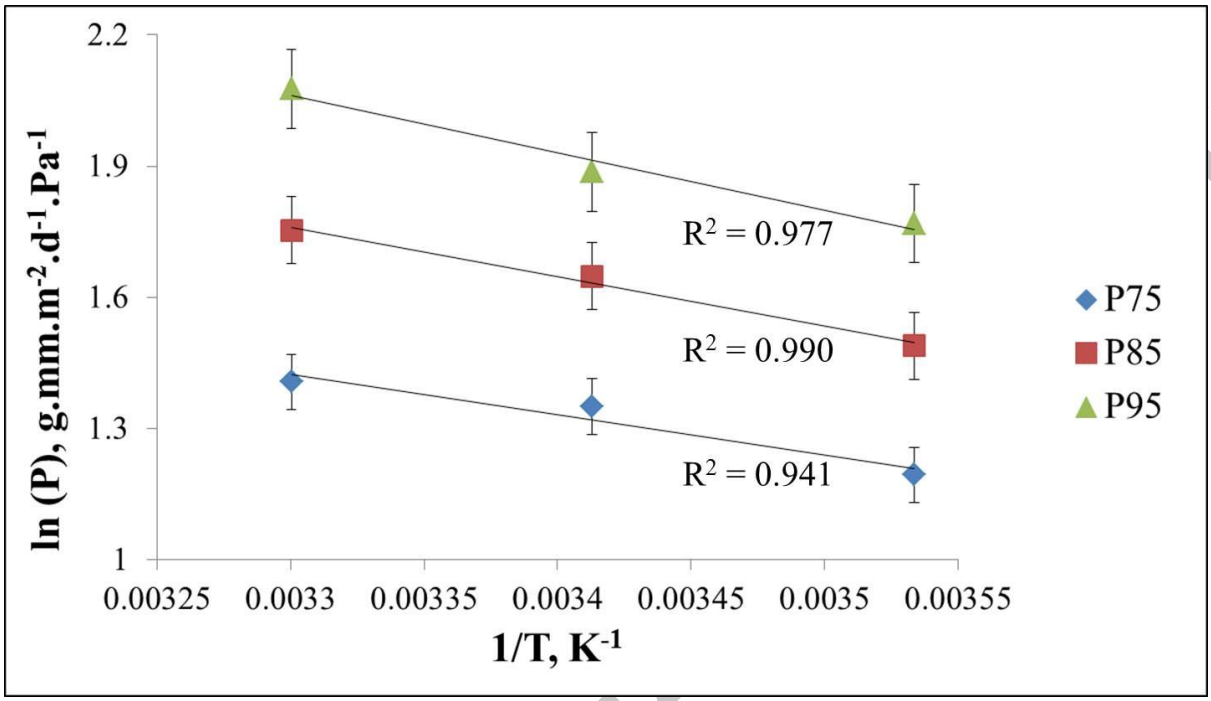

Fig 3 Arrhenius plot showing permeability effect on film moisture barrier properties as influenced by temperature-time dependence of WVP and predicted by Arrhenius models.

A rise in temperature resulted in increases in permeation for all RH tested (Table 2), which is also well-illustrated in Arrhenius model graphs by the linearity of the plots and best fits (Fig 3). The linearity confirms that water uptake is regulated by the diffusion process [20]. It has been reported that Arrhenius model allows for estimation of temperature shift factors by extrapolation, thereby being able to predict the lifespan of products [49]. A decrease in activation energy (E_a) of permeation and an increase in pre-exponential factor (P_o), proved a usual pattern of global (Arrhenius-type) model- dependency of temperature, and an activation energy independent of RH, with a pre-exponential factor varying exponentially (Table 2). The relatively low E_a at all RH (Table 2) compared to wheat gluten coating of 14.20 Kcal/mol (59.41 kJ/mol) [50], low density polyethylene and oriented polypropylene of 21.23 kJ/mol and 21.39 KJ/mol [51], implies that IBC films can be performed in applications that require relatively higher temperatures. This is interestingly good for IBC films, and shows the advantage of SRRC over other conventional processing methods. With Arrhenius model, the shelf-life of materials with temperatures close to and above their glass transition (Tg) can be estimated. In this study, films with Tg around 40^0C, corresponding to WVP test temperatures of 40^0C, were produced from intact bitter cassava, suggesting that the above model is applicable to IBC films.

3.2 Permeation to oxygen

The purpose of measuring oxygen transport through IBC films at three different temperatures and RH was meant to simulate their effect under supply chain conditions. The effect of temperature and RH on the permeability to oxygen (PO_2) is illustrated in Fig 4, showing that temperature had a highly significant ($p \leq 0.05$) positive impact, whereas RH had highly negative impact on PO_2. At any given temperature, an increase in RH caused a slight decrease in the permeation of the two gases, suggesting that moisture could be involved in

antagonising diffusion perhaps due to reductions in the size of voids. In a purposive pre-test trial (PPT) with micro-perforated biobased films, to determine package performance, it was apparent that increase in RH reduced gas permeation. Although the effect was not so much pronounced with the type of film used, this could pose challenges to the development of biobased films, particularly for those destined for packaging. The PPTs are sometimes carried out in vitro to gauge the direction of an experiment/study.

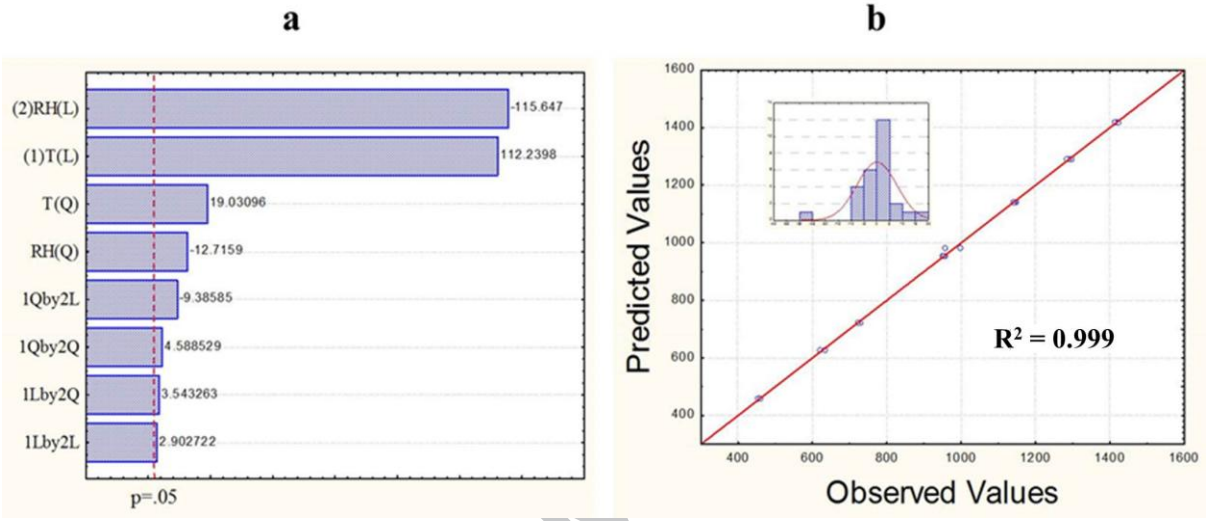

Fig 4. Effect of temperature and RH on the permeability to oxygen

The temperature-dependence permeability coefficients (PC) of oxygen (O_2) at 75 and 95 % RH in IBC films is shown in Table 3. In the 10-40 ^{o}C, films stored at 95 % RH exhibited highest O_2 permeation compared to those kept at 75 % RH. The observed behaviour might be due to increased molecular kinetics at high temperatures leading to water molecules interfering with film voids. The pre-exponential factors and activation energies were in the order of the PC: 75 % RH > 95 % RH. This could be explained by the interference of permeability to O_2 at higher RH. Furthermore, as the temperature increased in the lower RH (75 %), IBC glass transition temperature (Tg) and crystallinity (CRY) increased. By contrast, the increase in temperature at higher RH (95 %) caused a decrease in Tg, with CRY associated with temperature and RH increases. The two phenomena can be attributed to the transformation of crystalline into amorphous regions that caused decrease in permeability to O_2.

Table 3 Permeation of oxygen in relation to thermal properties of intact bitter cassava films

Gas	T, ^{0}C	RH, %	Thermal properties		P, cm^3 cm / (cm^2.s.cmHg)	A_t; RH, ^{0}C, %	P_{ef}, cm^3 cm / (cm^2.s.cmHg)	E_p, J/mol
			Tg	Cry, %				
O_2	10	75	38.70	52.28	7.66×10^{-5}	10–40; 75	1470.00×10^{7}	32.79
	40	75	40.20	60.63	2.02×10^{-5}			
	10	95	38.00	30.72	23.60×10^{-5}	10–40; 95	2.52×10^{7}	20.45
	40	95	36.70	55.45	10.27×10^{-5}			

T, temperature;, RH, relative humidity; P, permeation of oxygen; A_t, area of glass transition temperature; P_{ef}, pre-exponential factor of permeation, E_p, Activation energy for permeation.

According to Table 3, the PO_2 did not obey Arrhenius rule as temperature increased from 10^0C to 40^0C regardless of RH. Nonetheless, PO_2 followed Arrhenius rule when RH was increased to 95% at higher temperature (40 ^{0}C). The observed change of PO_2 at Tg suggest that PO_2 is influenced by a change in chain mobility. The PO_2 seems to be significantly influenced by RH, with reductions in permeation (Table 3). This supports the explanation provided earlier on the influence of moisture on the shape and perhaps size of voids in IBC films. Generally, the information provided is important particularly for the choice of deploying IBC films in commercial applications in which most polymer materials are applied below or above transition conditions [52]. Since IBC temperature dependence of PO_2 was not influenced by CRY at high RH is a good signal that IBC materials can be blended with other commercial polymers such polylactic acid (PLA) to deliver good quality materials under moisture-stressed environments. The temperature dependence of gas permeability of PLA has been reportedly not affected by transition conditions [52].

3.3 Mass transport characteristics of solvents through intact bitter cassava (IBC) films

The pattern of solvent diffusion through IBC films is shown in Fig 5. It can be clearly noted that there was lower moisture absorption at 75 % RH (Fig 5a) than 95 % RH (Fig 5b), causing lower swelling at 75% RH than at 95% RH; and a similar differences was also apparent for toluene (Fig 5c) and paraffin oil (Fig 5d) diffusions in the IBC films at 25^0C, 50 % RH. The higher swelling of IBC films in the 95% RH than in 75% RH could be due to higher plasticisation. With plasticisation, which is essentially an increase of the molecular relaxation time with higher water content, molecular mobility is easier the higher the water content and that would mean that the absorption/swelling would increase with the humidity.

Conversely, the nature of toluene and paraffin oil profiles might be due to the dilution effect [12] and, perhaps, the interaction effect of these solvents on IBC films (Table 4b). It might be that paraffin oil formed part of the film matrix and interacted more than toluene (as shown for χ values (Table 4b) or more oil adhered to the film and increased the mass, thus the higher values observed. In this study, paraffin oil was physically observed to cling to film surfaces even when the films were blotted prior to taking weights. The patterns of toluene and paraffin oil are similar to those that have been reported for these solvents through polymer gloves [25], implying that the latter and IBC films behave similarly. However, as compared to polymer gloves, the diffusion of toluene and paraffin oil through IBC films is faster.

Table 4 Film transport properties in different solvents at 25^0C, for IBC (a) and comparison of IBC film-solvent interaction with polymer glove's rubber-toluene interaction (b).

a

Solvents	Inst. Mass uptake, mg	Desorption rate, mg/min	FS_{ol}, mg/ml	FS_{tm}	δ_s g/cm^3	δ_f g/cm^3	R^2	n
Water 75	0.223	0.005	0.471	1.077	0.750	0.090	0.896	1.002
Water 95	2.560	0.027	3.975	10.616	0.950	0.090	0.932	0.997
*Toluene	$1.48x10^{-3}$	0.314	0.039	0.005	0.890	0.090	0.896	0.339
**Paraffin oil	$3.20 x10^{-6}$	0.001	0.081	0.076	$7.00x10^{-6}$	0.090	0.951	0.536

b

Material	χ	Reference
IBC film -75RH	0.357	This study
IBC film - 95RH	0.369	This study
IBC film-Toluene	0.342	This study
IBC film-paraffin oil	0.670	This study
Butyl rubber-Toluene	0.540	[20]
Nitrile rubber-Toluene	0.690	[20]
Natural rubber-Toluene	0.378	[38]

n, kinetic exponent associated with solvent transport characteristics; 75 & 95, relative humidity corresponding to water activities (0.75 & 0.95); stars (& **), values measure in micrograms (μg); χ, film-solvent interaction value.*

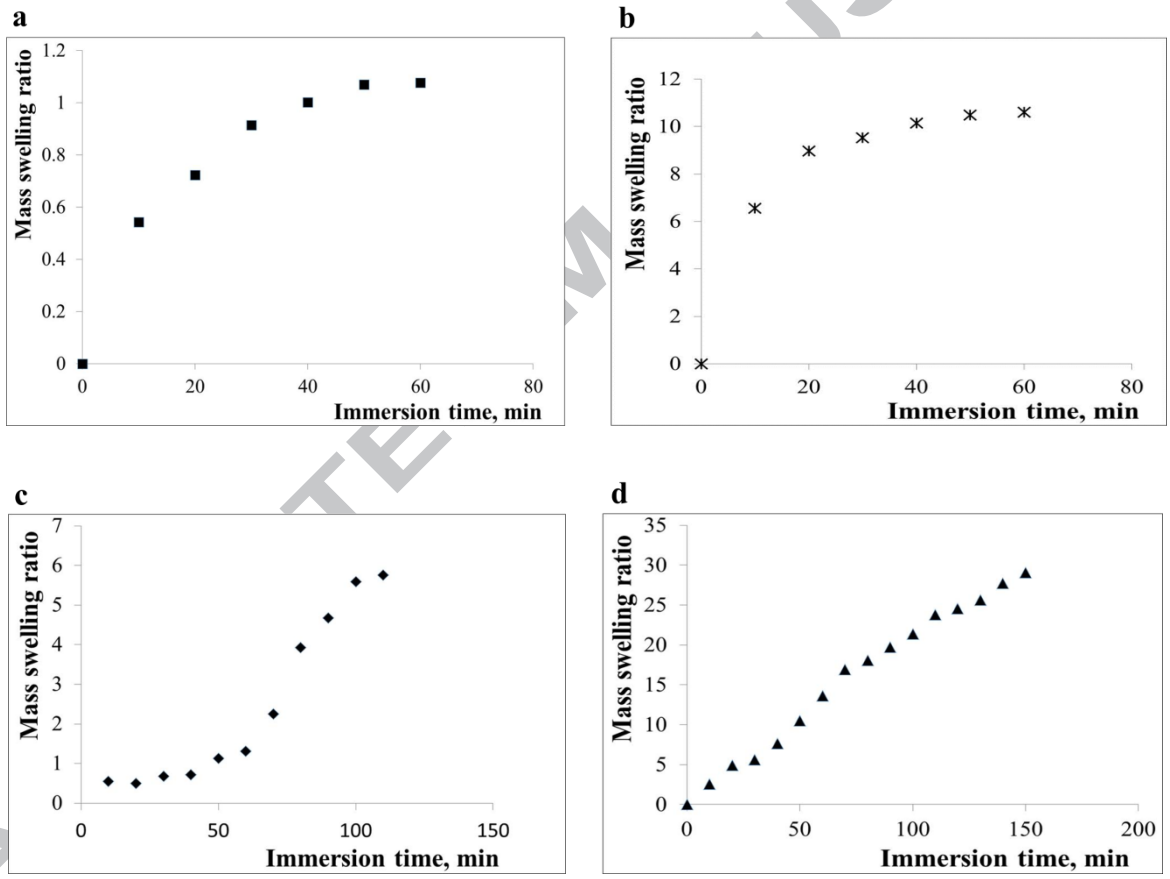

Fig 5 Comparison of the effect of solvents on swelling of IBC films. Water at 75 % RH (a), 95 % RH (b), toluene (c) and paraffin oil (d)

The swelling ratio patterns could be explained on the account of the viscous nature of the solvents. Although viscosity was not determined in this study during the experiment, paraffin oil showed high stickiness and low flow compared to toluene. In macromolecular network systems, fluid transport mechanisms through polymers are often described by diffusional kinetic exponents, which also describe Fickian and non-Fickian diffusional release from thin films [34]. Thus, the water at 75 % RH and 95 % RH through IBC films followed case II non-Fickian compared to Fickian diffusion exhibited by toluene and paraffin oil when

diffused through the film (Table 4a). The Fickian diffusion nature of IBC films is in agreement with what was observed with toluene penetration of rubbery polymers [25, 53].

Furthermore, the lower interaction factor of IBC films with water at 75 % RH and toluene imply that these two solvents cause less swelling compared to water at 95 % RH and paraffin oil (Table 4b). In comparison with butyl and nitrile rubbers, toluene causes more swelling to IBC films than to the former.

An initial steep film mass swelling front at 75% RH and 95% RH, yielding a weight gain proportional to time was perhaps due to their influence on the film molecular mobility causing faster crystalline to amorphous transformations. By contrast, the slow, and near constant film mass swelling fronts of toluene and paraffin oil respectively perhaps depended on their nature and activity. The toluene quite drastic increase in the swelling ratio after 50 min immersion might be related to its effect on the film molecular mobility causing faster crystalline to amorphous transformations. With toluene flowing through the film almost freely at this stage, it easily supplies the amounts needed for the swelling at the propagating concentration front or putting a sufficiently high stress on the film network for the swelling on strained chains. The film swelling pattern caused by paraffin oil could be attributed to its low molecular weight resulting in obeying type I diffusion, with a mass swelling increase proportional to the immersion time (54).

The profiles of mass transfer of organic (toluene) and inorganic (paraffin oil) solvents are illustrated in Fig 6, showing that toluene vapour transfer through the film is initially governed by case II diffusion up to saturation point (SP) in the first 80-100 mg (RP model) compared to experimental profile (EXP.) in the first 30-40 mg (Fig 6a). The mass transfer of paraffin oil vapour behaved similarly but with the case II diffusion occurring slightly higher (90-100 mg). According to Siepmann & Peppas, [55], when n value (Eq. 13) is 0.43, $0.43 < n < 0.85$, 0.89, and $n > 1.0$, the transfer behaviour of solvent diffusion mechanisms assume Fickian, anomalous (non-Fickian), case II, and super case II transport respectively. Thus, for the two solvents after SP, diffusion was governed by non-Fickian. It is widely known that case II diffusion occurs mainly in heterogeneous glass polymers arising from matrix swelling [56]. Like any other polymer, and based on this experiment, cassava behaves similarly. It is shown in Fig. 6a and 6b that the films absorbed more paraffin oil vapour than toluene vapour. This may be attributed to the more internal film stress, causing film to deform under the influence of high mobile paraffin oil in film matrix. The higher mass sorption results demonstrated by the RP model fitted data is an indication of the requisite to estimating accurate solvent mass sorption of films.

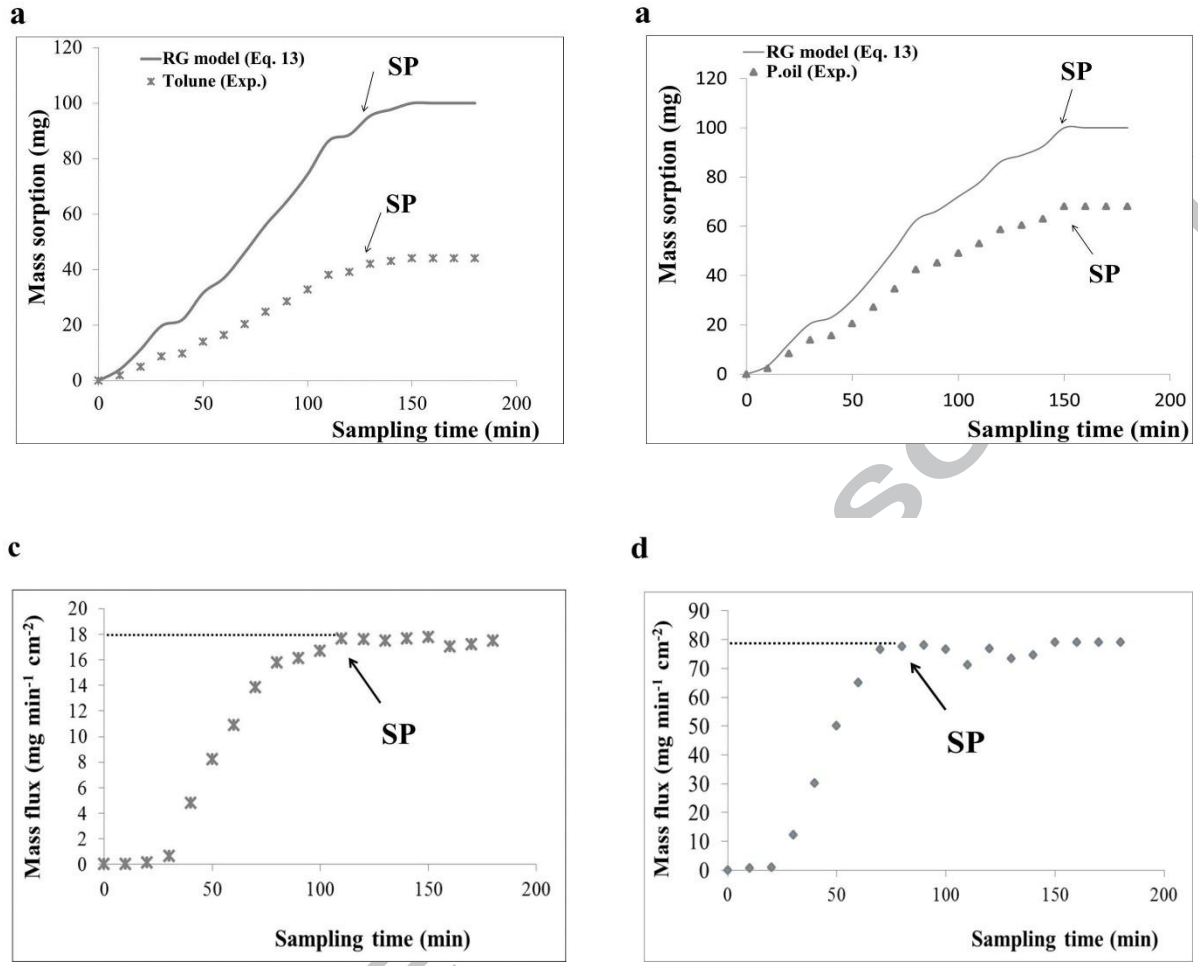

Fig 6 Mass sorption profiles of toluene vapour (a) and paraffin oil (b); and mass flux profiles of toluene (c) and paraffin oil (d) permeated through the film

The mass flux profiles for toluene (Fig 6c) and paraffin oil (Fig 6d) vapour through the film indicate that solvents permeation into films is directed by Fickian diffusion. Like in mass sorption, the faster time to reach SP, and the high SP mass flux for paraffin oil could be related to the strong stress imposed on the film by the solvent. The higher/steep increase in mass flux of paraffin oil after 20 min than toluene may be due to its higher mobility in the film accumulating more free volumes [56]. Accordingly, it can be said that the films need to be more protected from paraffin oil than toluene while both materials are applied in the distribution chain.

These results imply that IBC films behave like glassy polymer under the two solvents' stress reflecting generally low cohesion and disorderly hole structures characteristic of case II diffusional deformation as result of structural swelling [56]. The observed case II diffusion might also be due to thin membrane exhibited by the IBC films. The heterogeneity in these films confirms some level of modification imparted by SRRC. It has been reported that most commercial polymers are heterogeneous in nature [12]. This is a good indication of the potential of these films to be used in tandem with commercial products in contact with a range of organic solvents, e.g., oils, but with restricted water contact, such as dry products.
The lower mass swelling ratio of 75% RH exposed films than 95% RH ones demonstrate their better RH resistance. Similarly, the lower mass swelling ratio, mass sorption and mass

flux including longer time before SP show better solvent-resistance of toluene than paraffin oil exposed films.

3.4 Impact of solvent mass transfer on film structural changes

An understanding of the association between solvent absorption, diffusion, solubility and structural changes and modification of the film matrix is essential to ensuring safe handling in the distribution chain. Structural change is one of the approaches to assess the impact of permeants into the film material. As shown in Table 5, the broader transition from the glassy to the rubbery region caused by the 10^{o}C - 75 % RH solvent characterises IBC films having a wider distribution of crosslinking density and lower homogeneity of these networks [57]. The films penetrated with 40^{o}C- 95 % RH and 10^{o}C- 95 % RH showed a slight decrease in glass transition, which might be attributed to higher solvent concentration (Table 4) due to increased plasticisation and more flexibility. In this study, it was observed that Toluene permeation caused films to become more brittle, consistent with low solubility and low swelling (Table 4) and higher Tg and Tm (Table 5). This might be explained by the fact that toluene-treated films could be more chrystalline with decreased molecular relaxation, and thus the low solubility and higher T_g and $T_{m.}$

Table 5 Effect of solvents diffusion on thermal properties of IBC films

Solvents	**Tg, ^{0}C**	**Tm, ^{0}C**	**CRY, %**	**Enthalpy change, J/(gK)**
10^{0}C-75% RH	38.7 (36.3-41.2)	200.5	52.30	0.121
10^{0}C-95% RH	38.0 (37.5-38.6)	197.9	30.72	0.003
40^{0}C-75% RH	40.2 (40.0-40.1)	179.0	60.63	0.006
40^{0}C-95% RH	36.7 (36.8-38.8)	197.2	55.45	0.074
Toluene	56.8 (55.1-56.2	203.3	40.72	0.007
Paraffin oil	36.6 (36.5-36.7)	164.8	79.21	0.003

Furthermore, the enthalpy differences among the solvent-diffused films could be explained by their mobility (i.e., the plasticising effect of solvent absorbing). The higher enthalpy change of 10^{0}C-75% RH-diffused films could be due to the minimal molecular mobility (low plasticisation) of the film, creating a rigid structure that reflects the amount of energy absorbed.

Fourier transform infrared spectroscopy (FTIR) spectra of film-solvent interaction during the transfer process are presented in Fig. 7.

The O-H stretches around 3000 cm^{-1} in Fig 7a and 7b, shown by broad bands, imply that moisture was involved in film-water interaction. However, it could also imply that glycerol was also involved. In this study glycerol was used to obtain solutions of relative humidity of 75 and 95 %RH. Furthermore, the C-H stretch peaks high than 3000 cm^{-1} in Fig 7c and 7d point to the presence of organic solvents, and thus involvement of toluene and paraffin oil interactions.

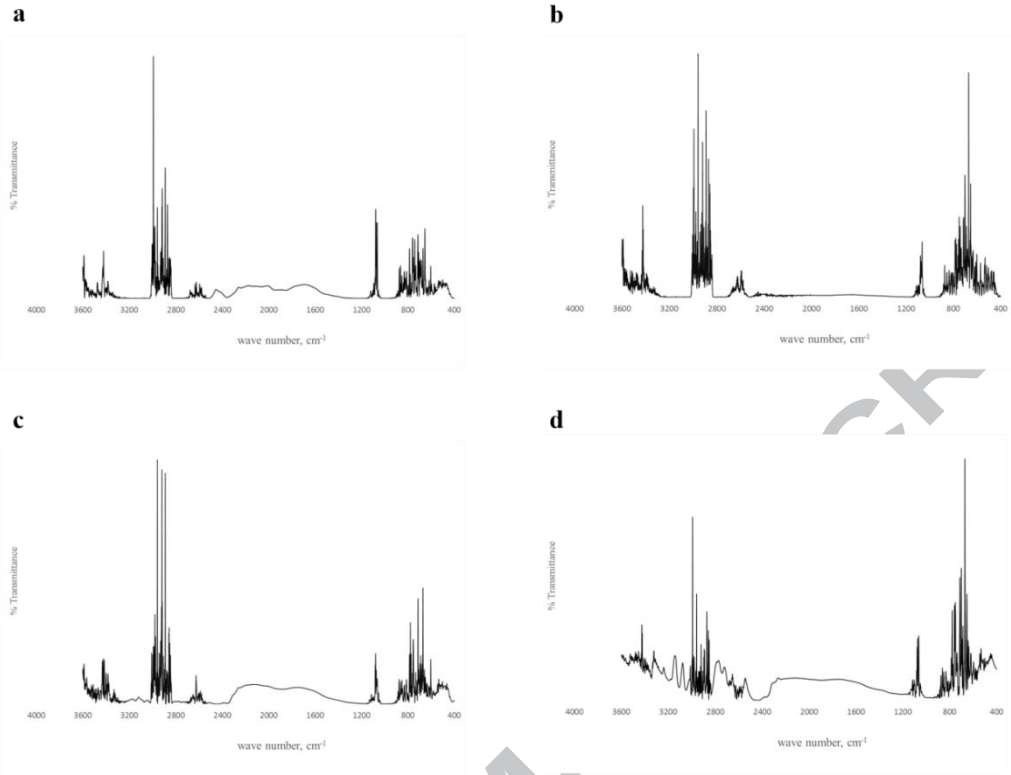

Fig 7 Effect of solvent diffusion on chemical properties of IBC films illustrated by FTIR Spectra of water at 75 % RH (a), water at 95 % RH (b), toluene (c) and paraffin oil (d)

Conclusions

Fluid transport phenomenon in humidity- temperature-stressed intact bitter cassava films has been assessed by qualitative and mechanistic techniques, and related to the structural characteristics of interactions.

The intact bitter cassava (IBC) films follow Type II isotherms. IBC film wide pore size distributions, causing tortuous and highly variable fluid pathways, suggests possible film-possession of wide variable permeability to fluids, which can be explored for packaging a broad spectrum of products. However, it also shows that care need to be taken to avoid constant exposure to high humidity.

By Modified BET, Peleg and Oswin models describing best equilibrium moisture content-water activity association at each temperature and under the conditions tested, implies that the models can be used as promising tools, to describe sorption behaviour of cassava biobased films.

For temperature and humidity increasing, exponentially, water vapour and oxygen permeation through IBC films, consistent with temperature dependence of Arrhenius concept, imply that film validation in targeted use conditions should be taken as a priority during biobased film package development.

With IBC film-solvent mass transfer mechanism, varying widely with time and 75-95 % RH, obeying case II non-Fickian, and toluene and paraffin oil following Fickian diffusion, it can be concluded that, like any other packaging films on the commercial markets, mass transfer in IBC films is governed by evaporation, diffusion, material solubility and interactions. Nonetheless, for effective determination of film swelling properties, the effect of the portion of the film solved in the different solvents should be considered in the experimental design.

Solvent-induced structural changes in IBC films, which were solvent-dependent, suggest that thermal and structural tests should be initiated concurrently with biobased materials during validation experiments.
The integrity of the cassava biobased film packages will depend on the host environment, and maximum care should be ensured to minimise its impact in the distribution chain. Nevertheless, CBF shows promise as potential food and non-food packaging application due to their self-sealing capacity, thermal stability, reasonable strength and transparent sheet [3] compared to current polymer packages.

Acknowledgements
The research fund support provided by World Bank via NARO EAAPP project is appreciatively recognised.

References

[1] J.H. Song, R.J. Murphy, R. Narayan, G.B.H. Davies, Biodegradable and compostable alternatives to conventional plastics. Phil. Trans. R. Soc. B, 364 (2009) 2127–2139.
[2] G.A. Arboleda, C.E. Montilla, H.S. Villada, G.A. Varona, Obtaining a Flexible Film Elaborated from Cassava Thermoplastic Starch and Polylactic Acid. Intern. J. Polym. Sc. (2015) 1- 9.
[3] K.S. Tumwesigye, J.C. Oliveira, M.J. Sousa-Gallagher, New sustainable approach to reduce cassava borne environmental waste and develop biodegradable materials for food packaging applications, Food Packag. Shelf Life, 7 (2016) 8–19.
[4] K. Marsh, B. Bugusu, Food Packaging—Roles, Materials, and Environmental Issues. J. Food Sci. 72(3) (2007) 1-17.
[5] A.R.V. Ferreira, V.D. Alves, I.M. Coelhoso, Polysaccharide-Based Membranes in Food Packaging Applications. Memb. (2016) 1-17.
[6] B. Imre, B. Pukánszky, Compatibilization in bio-based and biodegradable polymer Blends. Eur. Poly. J. 49 (2013) 1215–1233.
[7] H.R. El-Ramady, É. Domokos-Szabolcsy , N.A. Abdalla, H.S. Taha, M. Fári, Postharvest Management of Fruits and Vegetables Storage, in: Sustainable Agriculture Reviews, Lichtfouse (ed.), Springer, New York, 2015.
[8] M.M. Mekonnen, M. Pahlow , M.M. Aldaya, E. Zarate, A.Y. Hoekstra, Sustainability, Efficiency and Equitability of Water Consumption and Pollution in Latin America and the Caribbean, Sustain. 7 (2015), 2086-2112.
[9] R. Joffe, L. Rozite, A.Pupurs, Nonlinear behavior of natural fiber/bio-based matrix composites, in: C.L. Bonnie-Antoun, H. Jerry-Qi, G.P.Richard Hall, T.H. Lu (Eds.), Challenges in Mechanics of Time-Dependent Materials and Processes in Conventional and Multifunctional Materials, Springer, New York, 2013, pp. 131–137.
[10] S.C. George, S. Thomas, Transport phenomena through polymeric systems, Prog. Polym. Sci. 26 (2001) 985-1017.
[11] G. Choudalakis, A.D. Gotsis, Permeability of polymer/clay nanocomposites: A review, Eur. Polym. Journ. 45 (2009) 967–984.
[12] L.H. Cheng, M.J. Chen, W.H. Cheng, C.H. Lin, C.H. Lai, Mass transfer of toluene vapor through protective polymer gloves, J. Membr. Sci. 409-410 (2012) 180–190.
[13] F. Dubreuil, N. Elsner, A. Fery, Eur. Phys. Journ. E; 12(2) (2003) 215-221.
[14] P.C. Belibi, T.J. Daou, J.M.B. Ndjaka, B. Nsom, L. Michelin, B. Durand, A Comparative Study of Some Properties of Cassava and Tree Cassava Starch Films, Physic. Proced. 55 (2014) 220–226.
[15] A.C. Souza, R. Benze, E.S. Ferrão, C. Ditchfield, A.C.V. Coelho, C.C. Tadini, Cassava

starch biodegradable films: Influence of glycerol and clay nanoparticles content on tensile and barrier properties and glass transition temperature, LWT-Food Sci. Techn. 46 (1) (2012) 110–117.
[16] Y. Zhong, Y. Li, Effects of storage conditions and acid solvent types on structural, mechanical and physical properties of kudzu starch (Pueraria lobata)-chitosan composite films. Starch/Staerke, 63(9) (2011) 579–586.
[17] C.M.P. Yoshida, A.C.B.Antunes, C. Alvear, A.J. Antunes, An absorption model for the thickness effect in hydrophilic films, I. Journ. Food Sci. Techn. 40(1) (2005) 41–46.
[18] A.H. Bedane, Q. Huang, H. Xiao, M. Elc,. Mass transfer of water vapor, carbon dioxide and oxygen on modified cellulose fiber-based materials, Nordic Pulp and Paper Res. Journ. 27 (02) (2012) 409–417.
[19] W.M. Ni, The mathematics of diffusion, Philadelphia: siam, 82 (2011).
[20] N. Sultana, T.H. Khan, Water absorption and diffusion characteristics of nanohydroxyapatite (nha) and poly(hydroxybutyrate-co-hydroxyvalerate-) based composite tissue engineering scaffolds and nonporous thin films, J. Nanom. 2013, 8.
[21] P. Suppakul, B. Chalernsook, B. Ratisuthawat, S. Prapasitthi, N. Munchukangwan, Empirical modeling of moisture sorption characteristics and mechanical and barrier properties of cassava flour film and their relation to plasticizing–antiplasticizing effects, LWT-Food Sci. Techn. 50(1) (2013) 290–297.
[22] C.E. Chinma, C.C. Ariahu, J.O. Abu, Chemical composition, functional and pasting properties of cassava starch and soy protein concentrate blends, J. Food Sci. Techn. 50(6) (2013) 1179–1185.
[23] S. Mali, L.S. Sakanaka, F. Yamashita, M.V.E. Grossmann, Water sorption and mechanical properties of cassava starch films and their relation to plasticizing effect, Carbohy. Polym., 60(3) (2005) 283–289.
[24] A. Lazaridou, C.G. Biliaderis, N. Bacandritsos, A.G. Sabatini, Composition, thermal and rheological behaviour of selected Greek honeys, J. Food Eng. 64(1) (2004) 9–21.
[25] M.J.Chen, L.H. Cheng, T.P. Tseng, Y.S. Huang, C.H. Lin, C.H. Lai, Modelling the transport of toluene liquid in protective polymer gloves using a fluorescent dye-tracing technique, Eur. Polym. Journ. 66 (2015) 407–418.
[26] W. Xu, S.S. Que Hee, Influence of collection solvent on permeation of di-n-octyl disulfide through nitrile glove material, J. Haz. Mater. 151(2-3) (2008) 692–698.
[27] F. Cao, G.L. Amidon, N. Rodriguez-Hornedo, G.E. Amidon, Mechanistic Analysis of Cocrystal Dissolution as a Function of ph and Micellar Solubilization, Mol. Pharm. acs.molpharmaceut.5b00862(2016).
[28] S. Zhu, R.H. Pelton, K. Collver, Mechanistic modelling of fluid permeation, 50(22) (1995) 3557–3572.
[29] C. Cotten, J.L. Reed, Mechanistic analysis of multi-omics datasets to generate kinetic parameters for constraint-based metabolic models, BMC Bioinf. 14(1) (2013) 32.
[30] I. Reinas, J. Oliveira, J. Pereira, P. Mahajan, F. Poças, A quantitative approach to assess the contribution of seals to the permeability of water vapour and oxygen in thermosealed packages, Food Pack. Shelf Life, 7 (2016) 34–40.
[31] ASTME, Standard practice for maintaining constant relative humidity by means of aqueous solutions, ASTM, American Society for Testing and L\/laterials, 2 (2012) 5.
[32] ASTM E96/E96M-05, Standard Test Method for Water Vapor Transmission of Material, American Society for Testing and Materials, Philadelphia, 2005.
[33] Abdellatief, J. Butler, A. Teixeira, B. Welt, E. Mclamore, S. Shukla, Predictive Modeling of Oxygen Transmission Through Micro-perforations for Packaging Applications, J. Appl. Pack. Res. 7(2) (2015) 17–31.
[34] P.L. Ritger, N.A. Peppas, A simple equation for description of solute release I. Fickian

and non-fickian release from non-swellable devices in the form of slabs, spheres, cylinders or discs, J. Cont. Rel. 5(1) (1987) 23–36.

[35] M. Ochs, B. Lothenbach, H. Wanner, H. Sato, M. Yui, An integrated sorption-diffusion model for the calculation of consistent distribution and diffusion coefficients in compacted bentonite, J. Contam. Hydrol. 47(2-4) (2001) 283–296.

[36] R.A. Orwoll, P.A. Arnold, Polymer–solvent interaction parameter χ, in: Physical properties of polymers handbook, Springer, New York, 2007, pp. 233–257.

[37] A. Fallis, Permeability, Diffusivity, and Solubility of Gas and Solute Through Polymers, J. Chem. Inform. Model. 53(9) (2013) 1689–1699.

[38] S.A. Arrhenius, Chambers's encyclopaedia, George Newnes ed.., London, 1874.

[39] A.J. Marzocca, Evaluation of the polymer-solvent interaction parameter λ for the system cured polybutadiene rubber and toluene, Polym. Test. 29(1) (2010) 119–126.

[40] C.A. Finch, Chemical Modification and Some Cross-linking Reactions of Water-Soluble Polymers, in: C.A. Finch (Ed.), Chemistry and technology of water-soluble polymers, Springer, New York, 1983, pp. 81–111.

[41] G.M. Bristow, W.F. Watson, Cohesive energy densities of polymers. Part 1.—Cohesive energy densities of rubbers by swelling measurements. Trans. Faraday Soc. 54 (1958) 1731–1741.

[42] M. Barlkani, C. Hepburn, Determination of crosslink density by swelling in the castable polyurethane elastomer based on 1/4-cyclohexane diisocyanate and para-phenylene, Iran. J. Polym. Sci. & Tech, 1(1) (1992) 1–5.

[43] J. Burke, Solubility parameters: theory and application, in: J. Burke, ed.), The Book and Paper Group of the American Institute for Conservation, Waahington DC, 1984.

[44] J. Crank, The mathematics of diffusion, second ed., Oxford university press, New York, 1979.

[45] K. Canning, A. Co, Edge Effects in Film Casting of Molten Polymers, J. Plastic Film and Sheet. 16(3) (2000) 188–203.

[46] M.M.I. Chowdhury, M.D. Huda, M.A. Hossain, M.S. Hassan, Moisture sorption isotherms for mungbean (Vigna radiata L), J. Food Eng. 74(4) (2006) 462–467.

[47] A. Farahnaky, S. Ansari, M. Majzoobi, Effect of glycerol on the moisture sorption isotherms of figs. J. Food Eng. 93(4) (2009) 468–473.

48] D. Weinkauf, D.R. Paul, Effects of Structural Order on Barrier Properties, Barr. Polym. Struct. 423 (1990) 60–91.

[49] J.L. Sullivan, Creep and physical aging of composites, Compos. Sci. Techn. 39(3) (1990) 207–232.

[50] M.N. Kumar, Z. Yaakob,. Biobased Materials in Food Packaging Applications, in: S, Pilla (Ed.), Handbook of Bioplastics and Biocomposites Engineering Applications, Wiley Online Library, Massachusetts USA, 2011, pp. 121–159.

[51] R. Kulchan, W. Boonsupthip, P. Suppakul,. Shelf life prediction of packaged cassava-flour-based baked product by using empirical models and activation energy for water vapor permeability of polyolefin films, J.Food Eng. 100(3) (2010) 461–467.

[52] T. Komatsuka, K. Nagai, Temperature Dependence on Gas Permeability and Permselectivity of Poly(lactic acid) Blend Membranes, Polym. Journ. 41(5) (2009) 455–458.

[53]B.A. Miller-Chou, J.L. Koenig, A review of polymer dissolution, Prog. Polym. Sci. (Oxford), 28(8) (2003) 1223–1270.

[54] H.B. Hopfenberg, H.L. Frisch, Transport of organic micromolecules in amorphous polymers. Polym. Lett. 7 (1969) 405-409.

[55] J. Siepmann, N.A. Peppas, Modeling of drug release from delivery systems based on hydroxypropyl methylcellulose (HPMC). Adv. Drug Deliv. Rev. 64 (2012) 163–174.

[56] L. Masaro, X.X Zhu, Physical models of diffusion for polymer solutions, gels and solids, Prog. Polym. Sci. (Oxford), 24 (1999).
[57] Z. Petrovic, Polyurethanes from Vegetable Oils, Polym. Rev. 48(1) (2008) 109–155.

Quantitative and mechanistic analysis of impact of novel cassava-assisted improved processing on fluid transport phenomenon in humidity-temperature-stressed bio-derived films

K.S. Tumwesigye, J.C. Oliveira, M.J. Sousa-Gallagher

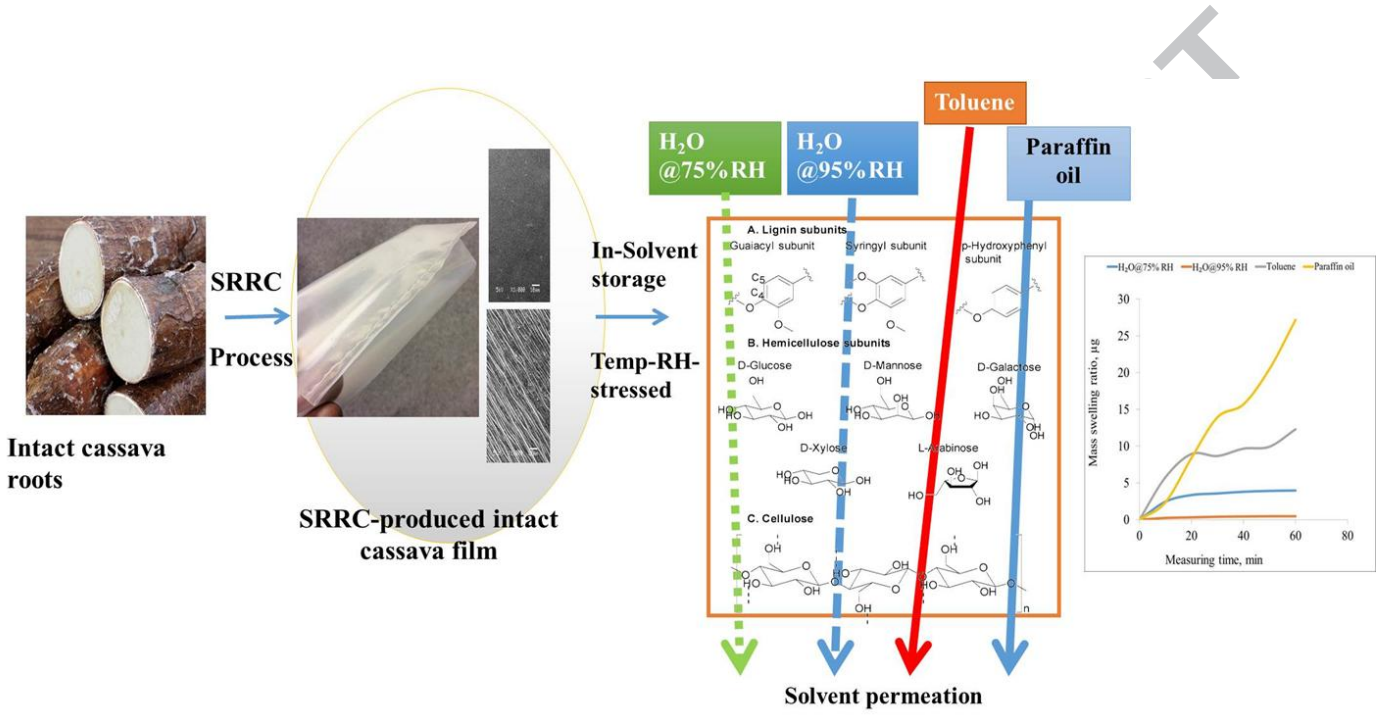

Highlights

- Intact bitter cassava film fluid transport behaviour in storage-stressed conditions
- Pore-size structure causes tortuous fluid pathways and variable permeability
- Fluid transport mechanisms obey mostly case II non-Fickian diffusion at high RH
- SRRC and stress-validation can assure film-resilience in strict tailor-use environs
- Qualitative-mechanistic study gives understanding of film fluid transport system